Nano Res. 2011, 4(11): 1129–1135
DOI 10.1007/s12274-011-0161-6
Research Article

ISSN 1998-0124
CN 11-5974/O4

Enhanced Electrical Properties in Carbon Nanotube/Poly (3-hexylthiophene) Nanocomposites Formed Through Non-Covalent Functionalization

Sung Hye Park[§], Sung Hwan Jin[§], Gwang Hoon Jun, Seokwoo Jeon (✉), and Soon Hyung Hong (✉)

Department of Material Science and Engineering, Korea Advanced Institute of Science and Technology, Daejeon 305-701, Republic of Korea

Received: 30 May 2011 / Revised: 28 June 2011 / Accepted: 30 June 2011

ABSTRACT

Poly(3-hexylthiophene) (P3HT) has received much attention as a good candidate to replace inorganic semiconductors for flexible electronics due to its solution-processability. However, the low charge mobility of P3HT is an obstacle to its commercialization. To overcome this problem, we propose a new non-covalent functionalization method for carbon nanotubes (CNTs) for use in CNT/P3HT nanocomposites. By using modified pyrene molecules with hydrophobic long alkyl chains, the non-covalently functionalized CNTs can become well dispersed in hydrophobic solutions and organic semiconductor matrices. Fabrication of organic thin-film transistors (OTFTs) from the non-covalently functionalized CNT/organic semiconductor nanocomposites shows that our non-covalent functionalization method significantly reduces damage to CNTs during functionalization when compared with covalent functionalization by treatment with acids. The OTFTs show 15 times enhancement of field effect mobility (1.5×10^{-2} cm^2/(V·s)) compared to the mobility of OTFTs made from pure P3HT. This enhancement is achieved by addition of only 0.25 wt% of CNTs to P3HT.

KEYWORDS

Carbon nanotubes, conjugated polymers, nanocomposites, organic thin film transistors

1. Introduction

Over the past decade, π-conjugated oligomeric, or polymeric, semiconducting materials have been suggested as good candidates to replace inorganic materials for flexible electronics because of their compatibility with solution processing. Solution-processability has numerous advantages such as large area coverage, structural flexibility, low-temperature processability, and low cost, [1–3]. Among these materials, regioregular poly (3-hexylthiophene) (P3HT) is one of the most promising conjugated polymers and is typically deposited by a solution process as an active material in organic thin-film transistors (OTFTs). P3HT has higher hole mobility than other solution-processed organic materials because of its good solubility in organic solvents and unique lamellar microstructure which influence charge transport via π–π stacked chains [4, 5]. However, spin-coated P3HT mostly exhibits low charge mobility due to the loss of crystallinity during the evaporation of solvents [6, 7].

In order to enhance its charge mobility, carbon

Address correspondence to Seokwoo Jeon, jeon39@kaist.ac.kr; Soon Hyung Hong, shhong@kaist.ac.kr
§ The first two authors contributed equally to this work.

nanotubes (CNTs) have recently been incorporated into P3HT. The advantage of CNT addition arises from their high aspect ratio, good conductivity, and excellent chemical stability in the matrix. Still, homogenous dispersion of CNTs in polymer is difficult to achieve because of the strong van der Waals interactions between them [8 ,9]. In order to realize the homogenous dispersion of CNTs in polymers, various functionalization schemes for CNTs have been proposed [10]. Covalent functionalization of CNTs by strong acids is a simple and general method to introduce functional groups onto the surface of CNTs [11–13], but it inevitably generates defects on the walls of CNTs during functionalization [14, 15]. These defects degrade the electrical properties of CNTs [16]. Recent studies of non-covalent functionalization [17–19] of CNTs by pyrene molecules open a new route to overcome the drawbacks of covalent functionalization. Pyrene molecules are planar conjugates having sp^2 structures like CNTs, and they are easily adsorbed on the surfaces of CNTs by π–π interactions. Various pyrene molecules, such as aminopyrene (AP) [17], pyrene carboxylic acid (PCA) [18], and pyrenebutyric acid (PBA) [19], enable the attachment of target functional groups onto CNTs without any damage to the CNTs. However, the hydrophilic functional groups in such pyrene molecules make it difficult to disperse CNTs in a hydrophobic matrix such as P3HT.

In this study, we propose a new non-covalent functionalization strategy for CNTs which uses modified pyrene molecules with long alkyl chains, which are sufficiently hydrophobic to be well-dispersed in P3HT. The non-covalently functionalized CNTs are successfully dispersed in a hydrophobic solution of P3HT. The introduction of functional groups and the attachment of modified pyrene molecules to CNTs are confirmed by Fourier transform infrared (FT-IR) and ultraviolet–visible (UV–vis) spectroscopy, respectively. Homogeneous dispersion states of CNTs in hydrophobic solvents are observed by scanning electron microscopy (SEM). Electrical conductivities of non-covalent functionalized CNT bucky papers are measured by 4-point probes. This showed conductivity one order of magnitude higher (809.9 S/cm) than that of covalently functionalized CNTs (75.9 S/cm). Fabrication of OTFTs using the non-covalently functionalized CNT/P3HT nanocomposites shows that this method significantly reduces damage to CNTs and the OTFTs show 15 times enhancement of field effect mobility (1.5×10^{-2} $cm^2/(V \cdot s)$) compared to the mobility of OTFTs made from pure P3HT. This enhancement is achieved by addition of only 0.25 wt% of CNTs to P3HT. This is the first example of the fabrication and characterization of CNT/P3HT OTFTs using non-covalently functionalized CNTs. For a similar fraction of CNTs in P3HT, the field effect mobility of CNT/P3HT OTFTs containing non-covalently functionalized CNTs is much higher than that of previously reported CNT/P3HT OTFTs which used covalently functionalized CNTs [20, 21].

2. Experimental

2.1 Synthesis of modified PBA (*m*-PBA)

PBA was modified as shown in Fig. 1. 50 mg of PBA was stirred in 20 mL of thionyl chloride ($SOCl_2$) containing 1 mL of dimethylformamide (DMF) at 70 ˚C for 12 h. After the remaining $SOCl_2$ was dried in a vacuum at room temperature, a mixture of the remaining solid and 1 g of octadecylamine (ODA) was stirred at 100 ˚C for 48 h and then washed with chloroform ($CHCl_3$) several times. After removal of solvents, the alkyl amide modified PBA (*m*-PBA) was obtained as a light yellow powder.

2.2 Preparation of functionalized CNTs

First, p-HiPco single walled CNTs (Unidym, USA) were added to HCl and sonicated for 12 h for purification. After washing with water, the CNTs were dried in a vacuum at 100 ˚C. After purification, 5 mg of CNTs were mixed with 50 mg of *m*-PBA and sonicated in $CHCl_3$ for 15 h. Then, the CNTs were washed with $CHCl_3$ three times. Finally, CNTs non-covalently functionalized by *m*-PBA (*m*-PBA–CNTs) were prepared by drying in a vacuum at 100 ˚C. Covalently functionalized CNTs were fabricated from purified CNTs (50 mg), which were added to conc. H_2SO_4 and conc. HNO_3 (3:1, 100 mL) solution and sonicated for three hours to induce oxidation. The covalently functionalized CNTs were washed until the washings had a pH of 7.

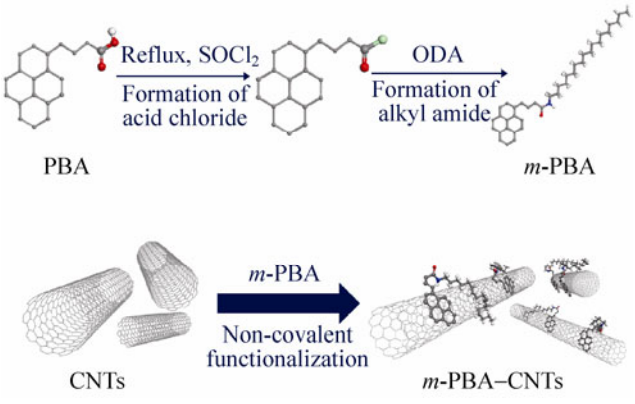

Figure 1 Schematic illustration of non-covalent functionalization of CNT by modified PBA which has alkyl amide functional groups (gray circles: carbon atoms, red circles: oxygen atoms, green circles: chlorine atoms, blue circles: nitrogen atoms)

2.3 Fabrication of CNT/P3HT nanocomposite OTFTs

The OTFTs were fabricated in a bottom gate configuration on highly doped n-type silicon (Si) substrates as the gate electrode with a 300 nm thermally grown silicon oxide (SiO_2) as the dielectric layer. The substrate was cleaned carefully, and hexamethyldisilazane (HMDS) was spin coated at 7500 rpm for 35 s CNTs with controlled concentrations (0.01, 0.1, and 0.25 wt% of *m*-PBA–CNTs and 0.01, 0.1, and 0.25 wt% of pristine CNTs with respect to P3HT) were sonicated for 30 min and then added to 0.5 wt% P3HT in chloroform. The solutions were spin coated at 2000 rpm for 60 s under an N_2 atmosphere inside a glove box, resulting in 50-nm-thick CNT/P3HT nanocomposites. Gold (Au) layers with 50 nm thickness were thermally evaporated on top of the semiconductor through a designed shadow mask in a vacuum chamber for the source and drain electrodes (channel width, W = 1500 μm, channel length, L = 100 μm).

2.4 Characterization

FT-IR spectra were recorded using the attenuated total reflectance (ATR) method (Jasco FT/IR-4100 type-A spectrometer) and UV–vis spectra were measured in THF solvents using a UV-3101PC spectrometer. The microstructure was analyzed by Hitachi S-480, SEM. High-resolution dispersive Raman microscope results were obtained from excitation by a 325 nm laser source (LabRAM HR UV/vis/NIR) and sheet resistances were measured by a 4-point probe (CMT-SR2000, AiT).

3. Results and discussion

Figure 1 is a schematic diagram showing the overall process of the non-covalent functionalization of CNTs with *m*-PBA. First, the carboxylic acid functional groups in PBA were converted to acyl chloride functional groups using thionyl chloride ($SOCl_2$) by acylation. Then, ODA with long alkyl chains was attached to the acyl groups of PBA by nucleophilic acyl substitution [21]. Finally, the *m*-PBA molecules, attached onto CNTs by π–π stacking, successfully functionalized CNTs non-covalently such that they become soluble in hydrophobic media because of the steric hindrance effect [22, 23] of the long alkyl chain attached to PBA.

The FT-IR spectra of the raw PBA, *m*-PBA, pristine CNTs, and *m*-PBA–CNTs non-covalently functionalized by *m*-PBA are shown in Fig. 2(a). The FT-IR spectrum of *m*-PBA shows the presence of three major signals at 2915 cm^{-1}, 2840 cm^{-1}, and 1660 cm^{-1}. The signals at 2915 cm^{-1} and 2840 cm^{-1} come from C–H stretching in alkyl chains, and the 1660 cm^{-1} signal indicates C=O stretching in amides. This clearly shows that the carboxylic acid functional groups of in PBA has been replaced by alkyl amide functional groups. After non-covalent functionalization, the *m*-PBA–CNTs show similar signals to *m*-PBA, while pristine CNTs do not exhibit any trace of signals. This evidence indicates that *m*-PBA is attached on the surfaces of CNTs without any damage to the functional groups. Figure 2(b) shows the UV–vis spectra for raw PBA, *m*-PBA, pristine CNTs, and *m*-PBA–CNTs. The spectrum of PBA has characteristic peaks at 266, 275, 327, and 344 nm, which arise from the π–π* transitions of pyrene rings [24]. Note that the spectrum of *m*-PBA shows broad peaks at 276 and 286 nm, which are similar to some of the PBA peaks. Compared to those of PBA, these peaks are slightly red-shifted due to the electronic intramolecular transitions between PBA and alkyl amide groups [25]. Furthermore, the spectrum of *m*-PBA–CNTs is much broader than that of *m*-PBA. These results show that *m*-PBA can promote the dispersion of CNTs by attaching to the CNTs. π–π interaction between *m*-PBA and CNTs is one possible reason for the formation of *m*-PBA–CNTs [17–19, 24]. Figures 3(a) and 3(b) show the characteristic dispersion

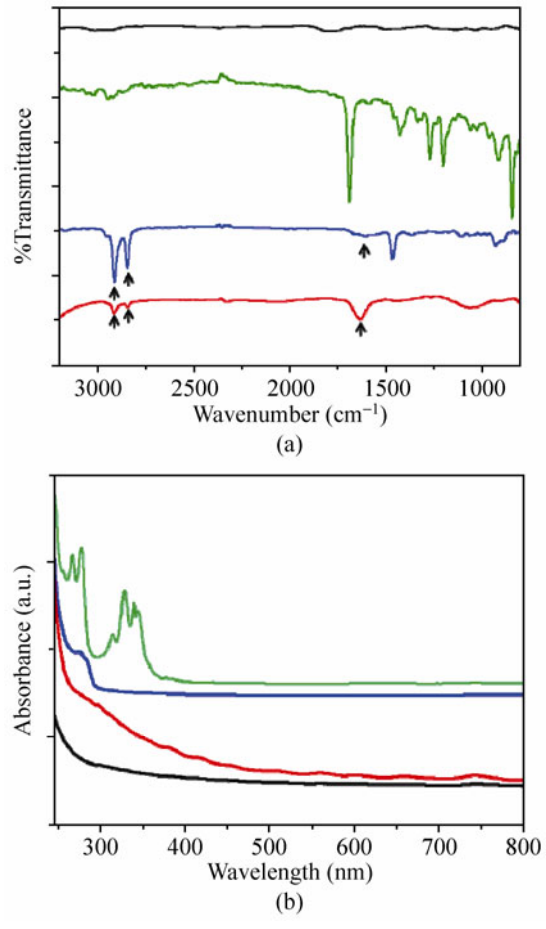

Figure 2 (a) FT-IR spectra and (b) UV–vis spectra for pristine CNT (black line), PBA (green line), modified PBA (blue line), and CNT non-covalently functionalized by *m*-PBA (red line)

states of CNTs in hydrophobic chloroform with (inset of Fig. 3(a)) and without *m*-PBA functionalization (inset of Fig. 3(b)) after 3 days of initial dispersion. SEM images of spin-coated pristine CNTs and *m*-PBA–CNTs dissolved in chloroform, followed by drying on a Si wafer, are shown in Figs. 3(a) and 3(b), respectively. Pristine CNTs remain highly bundled and agglomerated as they are in the solvent, while *m*-PBA–CNTs exhibit highly homogeneous dispersion. These results demonstrate that non-covalent functionalization of CNTs by *m*-PBA is an effective method to disperse CNTs in hydrophobic media. Resonance Raman spectroscopy is routinely used to investigate changes in the structure and properties of CNTs. Normalized resonance Raman spectra of pristine CNTs, *m*-PBA–CNTs, and covalently functionalized CNTs after strong acid treatment are shown in Fig. 3(c). The ratio between the D-band (sp^3) and G-band (sp^2) is related to the number of structural defects in CNTs. The D/G intensity ratio of *m*-PBA–CNTs (0.190) is similar to that of pristine CNTs (0.157), while that of covalently functionalized CNTs (0.380) is over twice that of pristine CNTs and *m*-PBA–CNTs. This indicates that non-covalent functionalization of CNTs by *m*-PBA

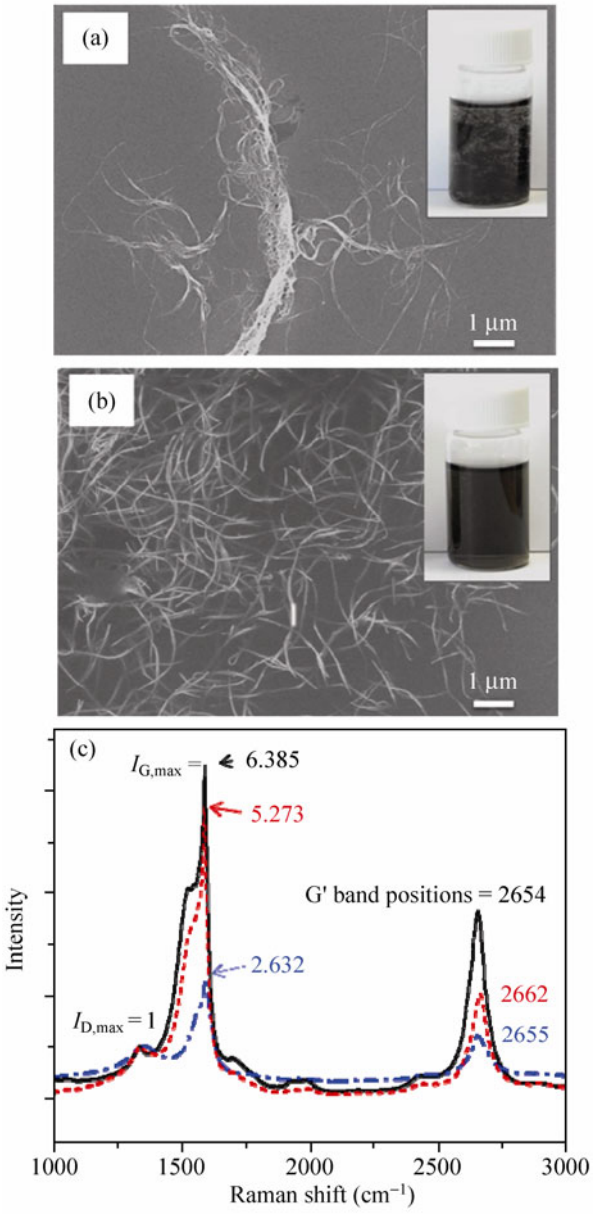

Figure 3 SEM images of (a) pristine CNTs, (b) *m*-PBA–CNTs on a Si wafer after dispersion in chloroform (inset images are digital photograph images of pristine CNTs and *m*-PBA–CNTs in chloroform after dispersion for several days), and (c) resonance Raman spectra of functionalized CNTs (black line: pristine CNTs, red line: *m*-PBA–CNTs, and blue line: covalently functionalized CNTs)

maintains the intrinsic properties of CNTs without introducing structural defects. In addition, the G′ band in *m*-PBA–CNTs has a higher Raman shift by 8 cm^{-1} compared to that of pristine CNTs. Because the G′ band is sensitive to charge transfer effects by absorbed species, upshift of the G′ band is indicative of electron transfer from the CNTs to pyrene molecules. This provides additional evidence of non-covalent functionalization of CNTs by *m*-PBA.

To evaluate the electrical conductivity and device performance of non-covalently functionalized CNTs, we fabricated CNT bucky papers (thin sheets of CNT aggregates) and CNT/P3HT OTFTs, respectively. CNT bucky papers were made from equal amounts of covalently functionalized CNTs and *m*-PBA–CNTs by filtering, and their electrical conductivities were measured by a 4-point probe (Table S-1 in the Electronic Supplementary Material (ESM)). The electrical conductivity of *m*-PBA–CNT is 10 times higher than that of the covalently functionalized CNT with the same amount of CNTs. To verify further, we fabricated a bottom-gate OTFT as shown in Fig. 4(a) and Fig. S-1 in the ESM. Figure 4(b) shows the output characteristics of pure P3HT, 0.25 wt% *m*-PBA–CNT/P3HT, and pristine CNT/P3HT devices at a gate bias voltage (V_{GS}) of –40 V. (Detailed information about output characteristics at various gate voltages for pure P3HT and *m*-PBA–CNT/P3HT devices as a function of CNT concentration and conductivity estimation of P3HT and CNT/P3HT devices are shown in Figs. S-2 and S-3 in the ESM, respectively.) The drain currents (I_{DS}) of devices consisting of CNT nanocomposites are higher than those of pure P3HT devices due to the addition of highly conductive CNTs. Furthermore, *m*-PBA–CNT/P3HT devices show much higher I_{DS} than pristine CNT/P3HT devices. This enhancement mostly results from the more homogeneous dispersion of *m*-PBA–CNTs in the P3HT matrix as compared to

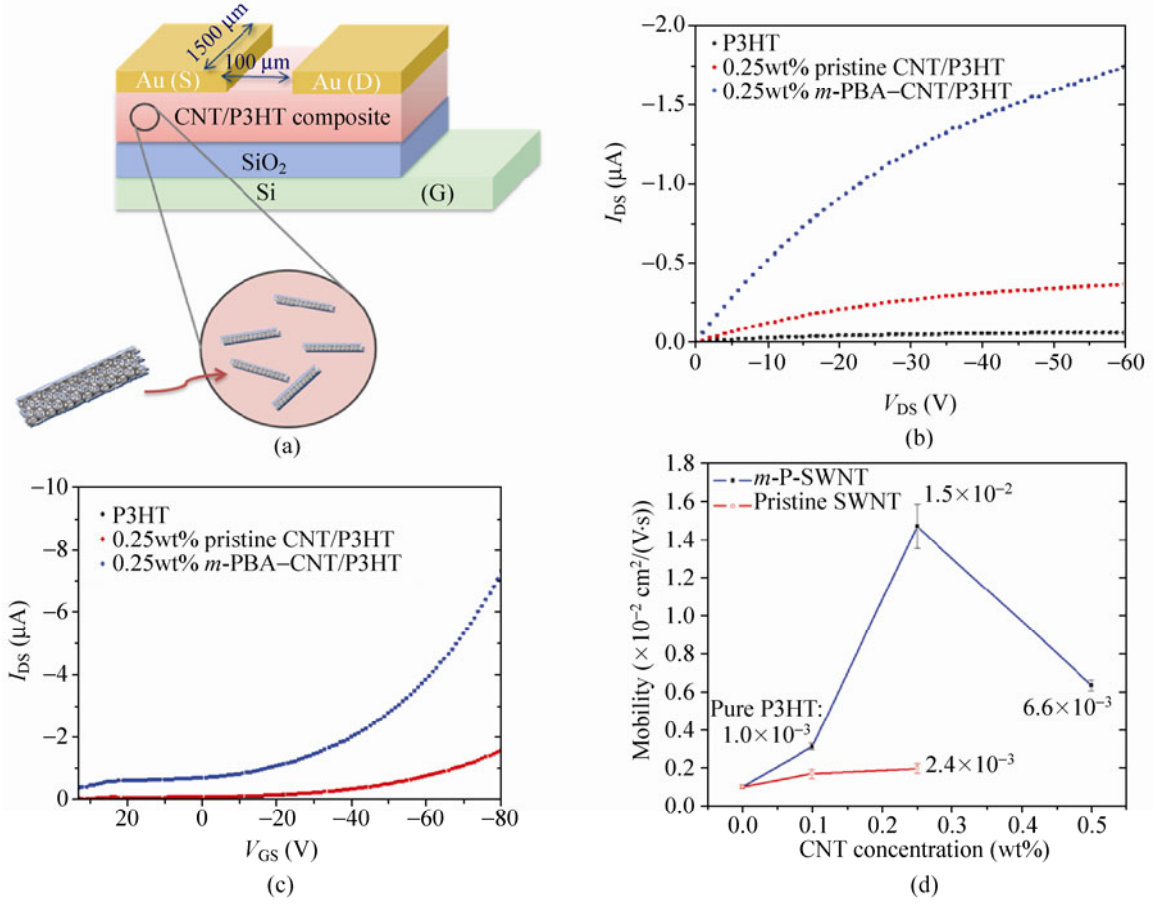

Figure 4 (a) Schematic view of the OTFT used in this work, (b) output characteristic curves, (c) transfer characteristic curves of OTFTs, and (d) field-effect mobility calculated for the samples as a function of the CNT concentration in the nanocomposites

pristine CNTs (Fig. S-4 in the ESM).

The average field-effect mobility of each transistor was calculated from the slope in the saturation region (drain voltage, V_{DS} = –80 V) from the transfer curves of devices as shown in Fig. 4(c), and the data were fitted to the following equation:

$$I_{DS} = \frac{W}{2L} C_i \mu (V_G - V_T)^2$$

where μ is the carrier mobility, and V_T is the threshold voltage (C_i = 10.8 × 10^{-9} F·cm^2, W = 1500 μm, and L = 100 μm). The field-effect mobility of the pure P3HT devices was 1.0 × 10^{-3} cm^2/(V·s). Pristine CNT/P3HT and *m*-PBA–CNT devices showed enhancement of field-effect mobility with increasing CNTs concentration. In particular, the field-effect mobility of *m*-PBA–CNT/P3HT devices was enhanced 15 times (to 1.5 × 10^{-2} cm^2/(V·s)) with 0.25 wt% addition of *m*-PBA–CNT in P3HT compared to pure P3HT devices. In contrast, the field-effect mobility of pristine CNT/P3HT devices was only 2.4 × 10^{-3} cm^2/(V·s) under the same conditions (Fig. 4(d)). This also reveals that *m*-PBA–CNTs serve more effectively as conducting pathways than pristine CNTs in a P3HT matrix. However, OTFT devices with over 0.25 wt% addition of non-covalent functionalized CNTs in P3HT showed lower mobilities (e.g., 6.6 × 10^{-3} cm^2/(V·s) for 0.5 wt% addition of *m*-PBA–CNTs) than 0.25 wt% addition of *m*-PBA–CNTs in P3HT. This mainly results from the agglomeration of CNTs in P3HT due to limited coverage of *m*-PBA molecules on CNTs at high concentrations of CNTs (0.5 wt% pristine CNT/P3HT devices do not show typical TFT behavior, and just show ohmic behavior due to the extensive agglomeration of CNTs in the P3HT matrix as shown in Fig. S-5 in the ESM).

4. Conclusions

We have systematically studied a new non-covalent functionalization of CNTs by using modified pyrene molecules with hydrophobic long alkyl chains. Non-covalently functionalized CNTs are well dispersed in hydrophobic solutions and a P3HT matrix. By using non-covalently functionalized CNT/P3HT a field effect mobility of 1.5 × 10^{-2} cm^2/(V·s) was achieved with only 0.25 wt% addition of CNTs in P3HT. Further non-covalent functionalization of CNTs and device performance should be studied for the realization or commercialization of CNT/polymer devices.

Acknowledgements

This research was supported by the Nano R&D program through the Korea Science and Engineering Foundation funded by the Ministry of Science & Technology (No. 2010-0019132). It was also partially supported by the Converging Research Center Program through the National Research Foundation of Korea (NRF) funded by the Ministry of Education, Science, and Technology (No. 2010-1079000) and supported by WCU (World Class University) program through the National Research Foundation of Korea funded by the Ministry of Education, Science and Technology (No. R32–10051).

Electronic Supplementary Material: Supplementary material (electrical conductivities of CNTs bucky papers, digital photograph image and SEM image of the OTFT device in this work, output characteristic curves of *m*-PBA–CNT/P3HT OTFTs and dispersion states of *m*-PBA–CNTs in a P3HT matrix) is available in the online version of this article at http://dx.doi.org/10.1007/s12274-011-0161-6.

References

[1] Murphy, A. R.; Frechet, J. M. J. Organic semiconducting oligomers for use in thin film transistors. *Chem. Rev.* **2007**, *107*, 1066–1096.

[2] Dimitrakopoulos, C. D.; Malenfant, P. R. L. Organic thin film transistors for large area electronics. *Adv. Mater.* **2002**, *14*, 99–117.

[3] Rogers, J. A.; Bao, Z.; Baldwin, K.; Dodabalapur, A.; Crone, B.; Raju, V. R.; Kuck, V.; Katz, H.; Amundson, K.; Ewing, J.; Drzaic, P. Paper-like electronic displays: Large-area rubber-stamped plastic sheets of electronics and microencapsulated electrophoretic inks. *Proc. Natl. Acad. Sci. U. S. A.* **2001**, *98*, 4835–4840.

[4] Reitzel, N.; Greve, D. R.; Kjaer, K. P.; Howes, B.; Jayaraman, M.; Savoy, S.; McCullough, R. D.; McDevitt, J. T.; Bjørnholm, T. Self-assembly of conjugated polymers at the air/water interface. Structure and properties of Langmuir and Langmuir–Blodgett films of amphiphilic regioregular

polythiophenes. *J. Am. Chem. Soc.* **2000**, *122,* 5788–5800.

[5] Österbacka, R.; An, C. P.; Jiang, X. M.; Vardeny, Z. V. Two-dimensional electronic excitations in self-assembled conjugated polymer nanocrystals. *Science* **2000**, *287*, 839–842.

[6] Tsukamoto, J.; Mata, J.; Matsuno, T. Organic field effect transistors using composites of semiconductive polymers and single-walled carbon nanotubes. *Jpn. J. Appl. Phys.* **2007**, *46*, 396–398.

[7] Park, Y. D.; Lim, J. A.; Jang, Y.; Hwang, M.; Lee, H. S.; Lee, D. H.; Lee, H. J.; Baek, J. B.; Cho, K. Enhancement of the field-effect mobility of poly(3-hexylthiophene)/functionalized carbon nanotube hybrid transistors. *Org. Electron.* **2008**, *9*, 317–322.

[8] Thess, A.; Lee, R.; Nikolaev, P.; Dai, H.; Petit, P.; Robert, J.; Xu, C.; Lee, Y. H.; Kim, S. G.; Rinzler, A. G.; Colbert, D. T.; Scuseria, G. E.; Tománek, D.; Fischer, J. E.; Smalley, R. E. Crystalline ropes of metallic carbon nanotubes. *Science* **1996**, *273*, 483–487.

[9] Ajayan, P. M.; Tour, J. M. Materials science: Nanotube composites. *Nature* **2007**, *447*, 1066–1068.

[10] Balasubramanian, K.; Burghard, M. Chemically functionalized carbon nanotubes. *Small* **2005**, *1*, 180–192.

[11] Cha, S. I.; Kim, K. T.; Arshad, S. N.; Mo, C. B.; Hong, S. H. Extraordinary strengthening effect of carbon nanotubes in metal-matrix nanocomposites processed by molecular-level mixing. *Adv. Mater.* **2005**, *17*, 1377–1381.

[12] Kuznetsova, A.; Mawhinney, D. B.; Naumenko, V.; Yates, J. T.; Liu, J.; Smalley, R. E. Enhancement of adsorption inside of single-walled nanotubes: Opening the entry ports. *Chem. Phys. Lett.* **2000**, *321*, 292–296.

[13] Ebbesen, T. W.; Hiura, H.; Bisher, M. E. Decoration of carbon nanotubes. *Adv. Mater.* **1996**, *8*, 155–157.

[14] Monthioux, M.; Smith, B. W.; Burteaux, B.; Claye, A.; Fischer, J. E.; Luzzi, D. E. Sensitivity of single-wall carbon nanotubes to chemical processing: An electron microscopy investigation . *Carbon* **2001**, *39*, 1251–1272.

[15] Yamamoto, G.; Suk, J. W.; An, J.; Piner, R. D.; Hashida, T.; Takagir, T.; Ruoff, R. S. The influence of nanoscale defects on the fracture of multi-walled carbon nanotubes under tensile loading. *Diamond Relat. Mater.* **2010**, *19*, 748–751.

[16] Zhang, X.; Sreekumar, T. V.; Liu, T.; Kumar, S. Properties and structure of nitric acid oxidized single wall carbon nanotube films. *J. Phys. Chem. B* **2004**, *108*, 16435–16440.

[17] Wang, S.; Wang, X.; Jiang, S. P. PtRu nanoparticles supported on 1-aminopyrene-functionalized multiwalled carbon nanotubes and their electrocatalytic activity for methanol oxidation. *Langmuir* **2008**, *24*, 10505–10512.

[18] Simmons, T. J.; Bult, J.; Hashim, D. P.; Linhardt, R. J.; Ajayan, P. M. Noncovalent functionalization as an alternative to oxidative acid treatment of single wall carbon nanotubes with applications for polymer composites. *ACS Nano*, **2009**, *3*, 865–870.

[19] Ham, H. T.; Choi, Y. S.; Chee, M. G.; Cha, M. H.; Chung, I. J. PEDOT-PSS/singlewall carbon nanotubes composites. *Polym. Eng. Sci.* **2008**, *48*, 1–10.

[20] Song, Y. J.; Lee, J. U.; Jo, W. H. Multi-walled carbon nanotubes covalently attached with poly(3-hexylthiophene) for enhancement of field-effect mobility of poly(3-hexylthiophene)/multi-walled carbon nanotube composites. *Carbon* **2010**, *48*, 389–395.

[21] Gan, Y.; Li, C. M.; Zhang, J.; Gamota, D. Organic thin-film transistors based on conjugated polymer/carbon nanotube composites. *Int. J. Nanotechnol*. **2007**, *4*, 441–449.

[22] Chen, J.; Hamon, M. A.; Hu, H.; Chen, Y.; Rao, A. M.; Eklund. P. C.; Haddon, R. C. Solution properties of single-walled carbon nanotubes. *Science* **1998**, *282*, 95–98.

[23] Hamon, M. A.; Hui, H.; Bhowmik, P.; Itkis, H. M. E.; Haddon, R. C. Ester-functionalized soluble single-walled carbon nanotubes. *Appl. Phys. A* **2002**, *74*, 333–338.

[24] Wu, X.; Shi, G. Synthesis of a carboxyl-containing conducting oligomer and non-covalent sidewall functionalization of single-walled carbon nanotubes. *J. Mater. Chem.* **2005**, *15*, 1833–1837.

[25] Pagona, G.; Tagmatarchis, N.; Fan, J.; Yudasaka, M.; Iijima, S. Cone-end functionalization of carbon nanohorns. *Chem. Mater.* **2006**, *18*, 3918–3920.